# Heterobarrier for converting hot-phonon energy to electric potential

Seungha Shin,[1] Corey Melnick,[1] and Massoud Kaviany[1,2,*]

[1]*Department of Mechanical Engineering, University of Michigan, Ann Arbor, Michigan 48109, USA*
[2]*Division of Advanced Nuclear Engineering, Pohang University of Science and Technology, Pohang, 790-784 Republic of Korea*

We show that hot phonons emitted in energy conversion or resistive processes can be converted to electric potential in heterobarrier structures. Using phonon and electron interaction kinetics and self-consistent ensemble Monte Carlo, we find the favorable conditions for unassisted absorption of hot phonons and design graded heterobarriers for their direct conversion into electric energy. Tandem barriers with nearly optical-phonon height allow for substantial potential gain without current loss. We find that 19% of hot phonons can be harvested with an optimized $GaAs/Al_xGa_{1-x}As$ barrier structure over a range of current and electron densities, thus enhancing the overall energy conversion efficiency and reducing waste heat.

## I. INTRODUCTION

Various decays, recombination, and drags in energy conversions and many resistive processes (e.g., in electronic circuits) emit phonons, hindering energy relaxation and transport in devices.[1–3] Among the phonon modes, energy relaxation through optical-phonon emission is dominant in semiconductors. Emission rate larger than decay can overpopulate the optical modes compared to their equilibrium population, and "hot phonons" represent this excess occupancy.[4] Examples include high-power electronic devices,[5] frustrated-vibration relaxation of chemisorbed molecules,[6] lattice electron stoppage of charged fission fragments,[7] and nonradiative decay of hot electrons in optoelectric devices.[8] These hot phonons are finally thermalized, converting their energy to waste heat and generating entropy. To improve the efficiency and mitigate heat generation, the thermalized phonons can be recycled by the anti-Stokes cooling (photo-assisted absorption of phonon), resulting in lower device operating temperatures.[9,10] Photonics including light emitting diodes show enhanced efficiency through thermoelectrically pumped heat.[11] However, utilizing the hot phonons before thermalization is expected to further improve the efficiency. Also, the removal of the excess phonon through this harvesting will lead to improved thermal management and device performance (reducing the phonon friction in electron transport).[12]

In this letter, we propose the unassisted absorption of hot phonons for direct electric potential gain using semiconductor heterobarriers. Barrier structures have been used in thermionics, thermoelectrics, and photovoltaics,[13–16] and for selective transmission of hot electrons (for thermoelectric performance enhancement) and heat absorption to restore the equilibrium electron distribution. Here, the heterobarrier structure is designed as an embedded structure rather than a stand-alone device, so that we can place the structure near the hot-phonon source for effective prethermalization harvesting. This requires kinetics optimization among the phonon absorption and emission (lifetime $\tau_{p\text{-}e}$) and up- and downconversion ($\tau_{p\text{-}p}$). The Monte Carlo method is employed to simulate this electron transport and phonon energy conversion in the diffusive regime, showing electric potential gain and phonon energy absorption.

## II. ANALYSIS METHODS

A heterobarrier structure composed of GaAs and $Al_xGa_{1-x}As$ ($x$ or $x_{Al}$ is the Al content) is chosen for this study. Since $Al_xGa_{1-x}As$ has a larger band gap than GaAs and the interface has a band-edge discontinuity in the conduction ($\Delta E_c = 0.79x_{Al}$, $x_{Al} < 0.41$) and valence bands ($\Delta E_v = -0.46x_{Al}$) depending on $x_{Al}$ (type I), the barrier height $\varphi_b$ can be controlled with $x_{Al}$.[17,18] We consider electrons as the main charge carriers and barriers in the conduction band. Potential barriers can cause an adverse (or reverse) current by reflection or potential change, so a large, forward local electric field formed by $x_{Al}$ grading is introduced in the barrier to compensate for this adverse effect.[14] Figure 1 shows the spatial distributions of (i) $x_{Al}$, (ii) electric field, $e_e$, (iii) product of electric potential and electron charge, $e_c\varphi_e$ (in conduction band edge), and (iv) optical and acoustic phonon temperatures, $T_{p,O}$ and $T_{p,A}$, in the hot-phonon absorbing barrier (HPAB) structure. The electric current density $j_e$, drift velocity $u_{e,d}$, and electron transition processes involving phonon absorption are also shown.

Interaction rates for the kinetics are calculated using the Fermi golden rule (FGR).[19] Because the single optical phonon interaction with an electron is based on a perturbation by the displacement $d$, the Hamiltonian with the $e$-$p$ interaction including the first-order perturbation is expressed as

$$H = H_o + H_{e\text{-}p} = (H_{e,o} + H_{p,o}) + \varphi'_{e\text{-}p}d, \quad (1)$$

where $H_o$ is the unperturbed Hamiltonian ($H_{e,o} + H_{p,o}$), and $H_{e\text{-}p}$ is the interaction Hamiltonian (with the first order $e$-$p$ coupling $\varphi'_{e\text{-}p}$, $H_{e\text{-}p} = \varphi'_{e\text{-}p}d$). Since the displacement $d = [\hbar/(2m\omega_{p,O})]^{1/2}(b^\dagger + b)$, where $m$ is the reduced mass of oscillating atoms, $\omega_{p,O}$ is the phonon frequency, and $b^\dagger$ ($b$) is the creation (annihilation) operator of phonon, the interaction rate from the FGR is expressed as

$$\dot{\gamma}_{e\text{-}p} = \frac{\pi}{m\omega_{p,O}}|\langle\psi_{e,f}|\varphi'_{e\text{-}p}|\psi_{e,i}\rangle|^2|\langle f_p \pm 1|b^\dagger + b|f_p\rangle|^2$$
$$\times \delta_D(E_{e,f} - E_{e,i} \mp E_{p,O}), \quad (2)$$

where $\psi_e$ is electron wave function, $f_p$ is phonon occupancy, $\delta_D$ is the Dirac $\delta$ function, and subscripts $i$ and $f$ represent the initial and final states. The interaction matrix
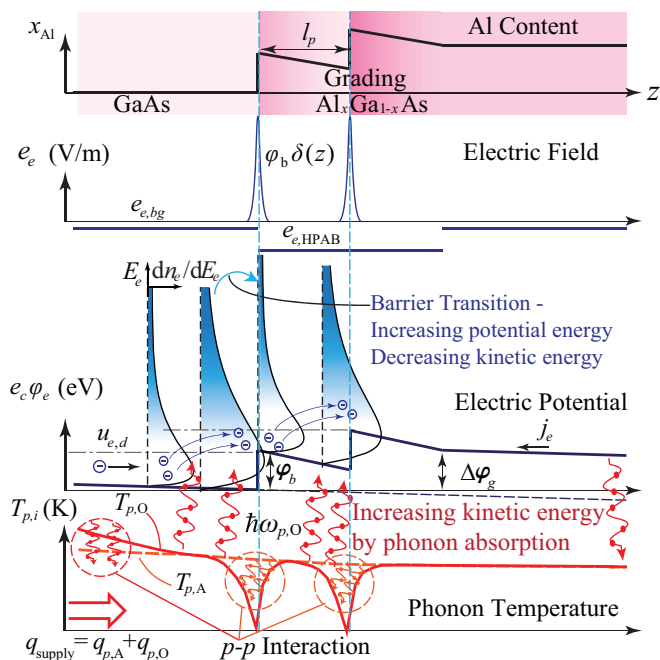
FIG. 1. (Color online) Spatial distributions of Al content, electric field and potential, and phonon temperatures in the hot-phonon absorbing barrier structure. $x_{Al}$ abruptly increases, creating the potential barrier (with height $\varphi_b$) in the conduction band edge, while the grading maintains the current. Phonon absorption populates electrons with higher energy than barrier height ($E_e > \varphi_b$) before or after the barrier transition, and this energy is converted to electric potential. The population of optical phonons quickly decreases at the barriers and recovers by upconversion.

element $|\langle \psi_{e,f}|\varphi'_{e-p}|\psi_{e,i}\rangle|^2$ for nonpolar optical phonon is $\phi'^2_{e-p}\delta_{D,\kappa}$, where $\phi'_{e-p}$ is the deformation potential and $\delta_{D,\kappa}$ is for the momentum conservation ($\kappa_{e,f} = \kappa_{e,i} + \kappa_p$, where

$\kappa_e$ and $\kappa_p$ are the electron and phonon momentum). For anisotropic polar optical phonon interaction, which absorbs or emits longitudinal optical (LO) phonon, the element becomes $(\rho e_c^2 \omega_p^2/\kappa_p^2)(1/\epsilon_{e,\infty} - 1/\epsilon_{e,s})\delta_{D,\kappa}$, where $\epsilon_{e,s}$ and $\epsilon_{e,\infty}$ are the static and optical dielectric constants, $e_c$ is the electron charge, and $\rho$ is the density.[20] Since $|\langle f_p \pm 1|b^\dagger + b|f_p\rangle|^2 = f_p + 0.5 \pm 0.5$, the phonon absorption and emission rates ($\dot{\gamma}_{p\to e}$ and $\dot{\gamma}_{e\to p}$) are proportional to $f_p$ and $f_p + 1$, respectively. From $\delta_D$ for the energy conservation, the phonon emission occurs only when the initial electron energy is larger than the emitted phonon energy ($E_{e,i} > E_{p,O}$), but the emission rate $\dot{\gamma}_{e\to p}$ increases with $E_e$ faster than the absorption rate $\dot{\gamma}_{p\to e}$. With higher $\varphi_b$, in order to pass through barriers, electrons require a larger momentum or $E_e$, or the less energetic electrons need to increase their energy through phonon absorption. However, high-energy carriers are emission-favorable and less populated, and multiphonon absorption for low-energy electron transition is not probable.[21] Thus, tandem-barrier structures with $\varphi_b \leqslant E_{p,LO}$ ($\approx$35 meV, only absorption available), rather than a single barrier with large height, are employed for large potential gain.

The lowest conduction band in GaAs has three valleys, at $\Gamma$, $L$, and $X$, where $\Gamma$ is heavily populated at room temperature. Electrons in the band are scattered through various mechanisms, and the overall interaction rates are shown in Fig. 2(a). The $\Gamma$-valley polar optical phonon interaction, which absorbs or emits longitudinal optical (LO) phonon, dominates for low $E_e$, and intervalley scattering is dominant when $E_e > \Delta E_{\Gamma L}$ (energy difference between $\Gamma$ and $L$ valleys). Average absorption $\langle \dot{\gamma}_{p\to e} \rangle$ and emission $\langle \dot{\gamma}_{e\to p} \rangle$ rates for $\Gamma$ valley is obtained considering LO phonon temperature $T_{p,LO}$ ($= E_{p,LO}/\{k_B[\ln(f_{p,LO} + 1) - \ln(f_{p,LO})]\}$) and electron distribution $dn_e/dE_e$ ($D_e f_e^o$, where $D_e$ is the density of states and $f_e^o$ is the equilibrium electron distribution), and favorable absorption and emission are also shown in Fig. 2(b).
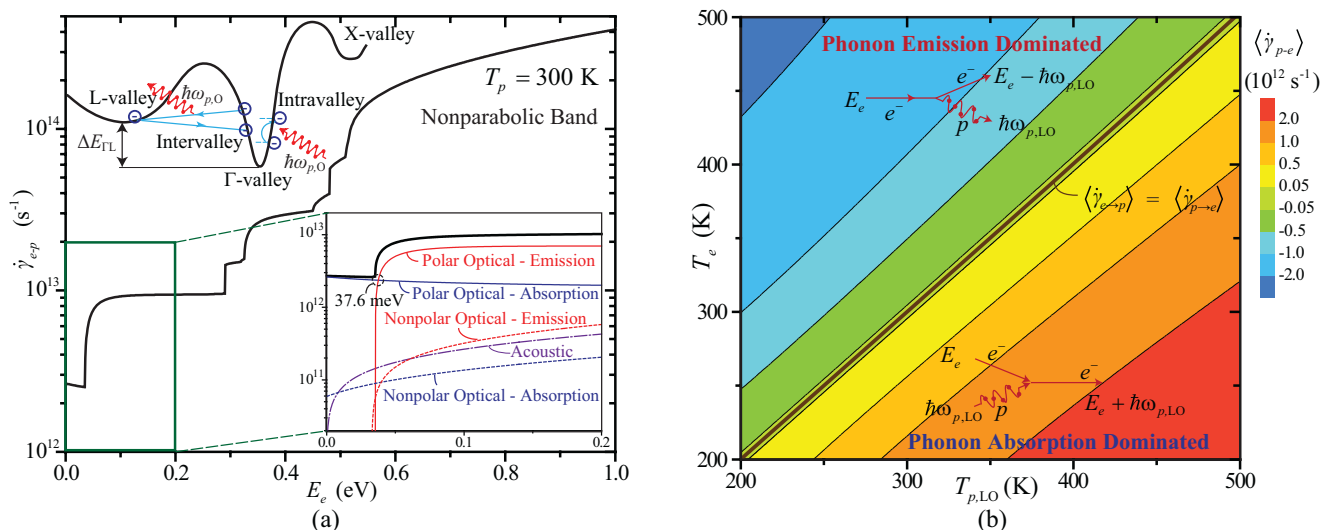


FIG. 2. (Color online) (a) Variations of the electron interaction rates in the lowest conduction band, as a function of electron energy ($E_e$) for $T_p = 300$ K. Insets show the band structure and various interaction mechanisms (left) and the interaction rates for low-$E_e$ $\Gamma$-valley electrons (right). Polar optical phonon scattering is dominant at low $E_e$, and intervalley scattering rates increase with $E_e$. (b) Average polar optical phonon absorption ($+$)/emission ($-$) rates as functions of $T_e$ and $T_{p,LO}$. The phonon absorption or emission rate becomes faster as nonequilibrium between electron and phonon increases.

The rate of three-phonon ($p$-$p$) interactions (up- and downconversion), competing with the $e$-$p$ interactions, are given by[22]

$$\dot{\gamma}_{p\text{-}p,\text{down/up}} = \frac{\hbar}{8\pi\rho^3} \frac{|M_{p\text{-}p}|^2 R}{u_{p,\text{A}}^7 u_{p,\text{O}}^2} \omega_{p,\text{A}}^2 \omega_{p,\text{O}}^3 [f_p(\omega_{p,\text{A}})$$
$$+ 0.5 \pm 0.5]^2 [f_p(\omega_{p,\text{O}}) + 0.5 \mp 0.5], \quad (3)$$

where $u_{p,\text{A}}$, $u_{p,\text{O}}$, $\omega_{p,\text{A}}$, and $\omega_{p,\text{O}}$ are the acoustic and optical phonon speeds and frequencies, $|M_{p\text{-}p}|^2$ is $4\rho^2\gamma_G^2 u_{p,\text{A}}^2 u_{p,\text{O}}^2$, $\rho$ is the density, $\gamma_G$ is the Grüneisen parameter, and $R$ is obtained from the force constants estimated by material metrics in Ref. 23. (With $\rho_{\text{GaAs}} = 5317$ kg/m$^3$, $u_{p,\text{A}} = 2800$ m/s, $\gamma_G = 0.8$, and $R = 0.128$, $\dot{\gamma}_{p\text{-}p}$ is 4.3 ps at 300 K, which agrees well with the experiments in Refs. 24 and 25.) Since the $e$-$p$ interaction rate is faster than the $p$-$p$, the electron is first excited and relaxed to equilibrium during the hot-phonon relaxation, and thus within a ps, it has large population at high $E_e$ (desirable for barrier transition). Thus, considering this downconversion of optical phonons along with their low mobility, HPAB placed near the phonon source is suited for harvesting hot phonons.

Self-consistent ensemble Monte Carlo (MC) simulates the electron transport and phonon absorption and emission in HPAB with large ensemble of sampled electrons coupling to the Poisson equation to reflect the internal charge redistribution.[26–28] The simulation includes acoustic, inter-, and intravalley optical phonon scatterings in the lowest conduction band and employs GaAs properties (effective mass $m_{e,e}$, dielectric constants $\epsilon_{e,\infty}$ and $\epsilon_{e,s}$, deformation potential $\phi'_{e\text{-}p}$, etc.),[20,29] as the small $\varphi_b$ requires a small change of $x_{\text{Al}}$ and physical properties ($\sim$4% change of $x_{\text{Al}}$ per barrier). The predicted electron mobility $\mu_e$ agrees well with experiments for bulk GaAs ($\mu_{e,\text{GaAs}} = 0.85$ m$^2$/V-s for low $e_e$ and decreases with $e_e$) for all electric fields,[30] verifying the algorithm. Sampled electrons travel with the prescribed electric potential along $z$ as described in the legend of Fig. 1 (the particle distribution in the lateral directions is not considered). Initially, 200 000 electrons over 1-$\mu$m region are sampled, and various numbers of barriers $N_b$ are placed with barrier pitch $l_p$ in the center. Particles are initially in $\Gamma$ valley, according to the equilibrium distribution with $T_e$. An appropriate background electric field $e_{e,bg}$ is applied to create a reference current density $j_{e,o}$ (or drift velocity $u_{e,d,o}$) without barrier, and a higher local electric field $e_{e,\text{HPAB}}$ (from the $x_{\text{Al}}$ grading) is applied to the barrier region. The $z$-direction boundaries are assumed to have constant charge distribution, and electrons are supplied to compensate for those exiting.

To maintain the phonon population (depends on $T_p$ through the Bose-Einstein distribution), phonon flux sufficient for the absorption over the simulation region is prescribed at the left boundary. Phonon transport and distribution are also simulated along with electrons through the phonon conductivity ($k_p$), $e$-$p$ interaction rates (for phonon absorption and emission, $\dot{\gamma}_{p\to e}$ and $\dot{\gamma}_{e\to p}$), and $p$-$p$ up- and downconversion rates ($\dot{\gamma}_{p\to p,\text{up}}$ and $\dot{\gamma}_{p\to p,\text{down}}$).[31] Because the hot phonon effect is prominent only in the LO phonon mode,[32] the conservation of the LO phonon (dominant in phonon absorption) and all other phonon modes (A) are separately tracked in each bin. Over the spatial increment ($\Delta z = 5$ nm), the phonon energy change (per area)

in the $j$th bin ($z_j$) over a time step ($\Delta t, t \sim t + \Delta t$) is

$$\Delta E_{p,i}(z_j) = \Delta t\{-(q_{p,i,L} + q_{p,i,R})$$
$$+ [\dot{s}_{e\text{-}p,i}(z_j) \pm \dot{s}_{p\text{-}p,\text{up}}(z_j)]\Delta z\}, \quad (4)$$

where $i$ is a phonon mode (LO or A; + for LO and − for A), and $q_{p,i,R}$ (or $q_{p,i,L}$) is the phonon flux from the neighboring bins, determined by $T_{p,i}$ and $k_{p,i}$ ($k_{p,\text{A}} = 54$ W/K-m and $k_{p,\text{LO}} = 1$ W/K-m, approximated from Ref. 33) as

$$q_{p,i,R \text{ or } L} = \frac{k_{p,i}}{\Delta z}[T_{p,i}(z_j) - T_{p,i}(z_j \pm \Delta z)]. \quad (5)$$

$q_{p,i,L}$ at the left boundary is prescribed ($q_{\text{supply}}$ is set to total phonon absorption), and $q_{p,i,R}$ on the right is calculated using an external thermal resistance (equivalent to 20 $\mu$m of GaAs) and the surrounding temperature ($T_o$). $\dot{s}_{e\text{-}p,i}$ and $\dot{s}_{p\text{-}p,\text{up}}$ depend on the electron distribution and phonon temperatures and are found from MC simulation and Eq. (3). Using $\Delta E_{p,i}$, heat capacity ($c_{p,i}$),[34] and LO phonon energy, the spatial distributions of $T_{p,\text{A}}$ and $T_{p,\text{LO}}$ are updated.

In barrier transition, electrons lose (forward) or gain (backward) momentum corresponding to $\varphi_b$ with the nonconserving lateral momentum,[15,35] and tunneling is not considered. With the lateral momentum conservation, smaller barrier transition efficiency is expected. Although epitaxial planar GaAs/AlGaAs heterostructures have shown that lateral momentum is mostly conserved, introducing surface roughness is expected to break the conservation and enhance the barrier transition.[35,36] The Fermi level, away from the HPAB, has the same distance from the band edge, due to the same level of doping and electron distribution. The potential gain through each barrier structure is estimated as $\Delta\varphi_{g,o} = \varphi_b + e_{e,\text{HPAB}}l_p$ (when the internal field by charge redistribution is not significant), and total potential gain is proportional to the number of barriers ($\Delta\varphi_g = N_b\Delta\varphi_{g,o}$). Note that $\Delta\varphi_g$ increases the required $x_{\text{Al}}$, which changes the properties (increase in the optical phonon energy $E_{p,\text{LO}}$ and decrease in the electron mobility $\mu_e$ due to larger $m_{e,e}$ and intervally scattering). Our simulation results with GaAs properties can be more safely accepted for lower $\Delta\varphi_g$. Properties from simulations (e.g., electron and phonon distribution, drift velocity, temperatures, and phonon absorption rate) are obtained by the ensemble average of the sampled particles from 0.5 to 1 ns.

### III. RESULTS AND DISCUSSIONS

The MC simulations demonstrate that the HPAB produces electric potential gain without current loss through a proper combination of the local barrier electric field ($e_{e,\text{HPAB}}$), the optical phonon population ($f_{p,\text{LO}}$), and the barrier height ($\varphi_b$), and the potential energy gain is based on phonon absorption. Since the adverse current caused by the barrier decreases with increasing $f_{p,\text{LO}}$ (or $T_{p,\text{LO}}$) due to large phonon absorption rate [as in Fig. 2(b)], larger $\Delta\varphi_g$ with smaller $e_{e,\text{HPAB}}$ can be achieved at higher $T_{p,\text{LO}}$. However, a large phonon population also increases the scattering rate, thus decreasing $\mu_e$. Acoustic phonons do not contribute to electron upconversion, so low $T_{p,\text{A}}$ and high $T_{p,\text{LO}}$ are desirable. With constant $T_{p,\text{A}}$ and $T_{p,\text{LO}}$, HPAB operating under high $T_{p,\text{LO}}$ has smaller current loss and larger $\Delta\varphi_g$ compared to the thermal equilibrium system. (Nonequilibrium $T_{p,\text{LO}} = 325$ K and $T_{p,\text{A}} = 300$ K
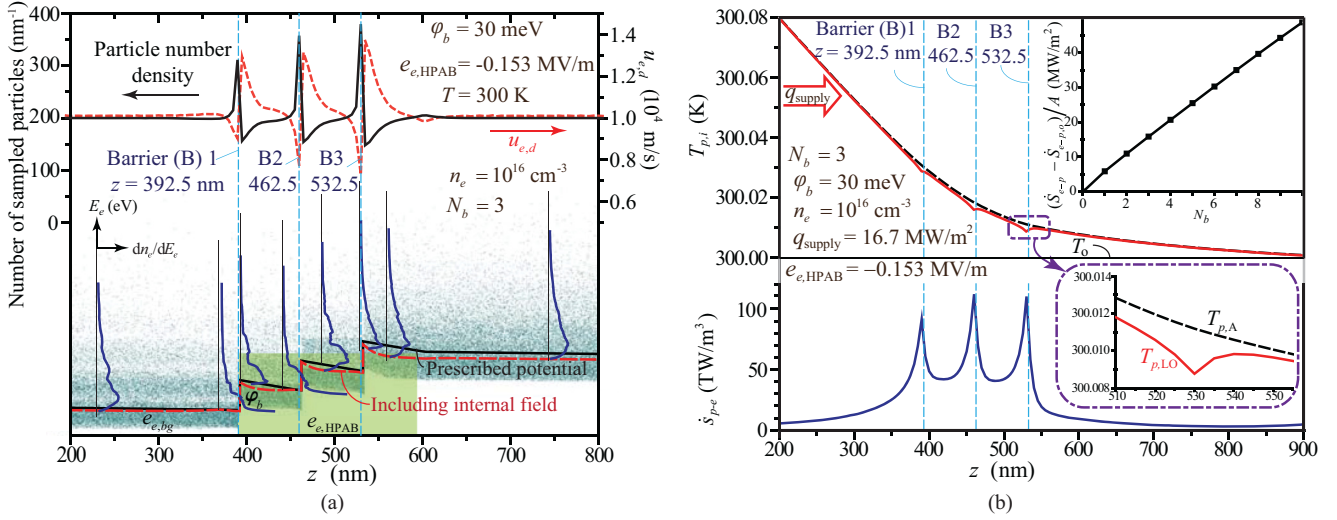
FIG. 3. (Color online) (a) Sampled particle number density, drift velocity ($u_{e,d}$), and particle-energy distributions over the simulation cell. Electrons are accumulated behind barriers and low-energy electrons are highly populated near barriers. (b) Distributions of phonon temperatures ($T_{p,A}$ and $T_{p,LO}$) and phonon energy absorption rate ($\dot{s}_{p\text{-}e}$). Large phonon absorption occurs around the barriers because of the large population of low-energy electrons, and this leads to the extended nonequilibrium between phonon modes. The total phonon absorption rate in HPAB ($\dot{S}_{p\text{-}e}/A$) is proportional to the number of barriers, as in the inset (top right).

in GaAs relaxes to an equilibrium temperature of 304 K from the energy conservation, and $\Delta\varphi_{g,o}$ reduces from 20.03 to 19.57 meV. Barrier transition is more effective in hot phonon systems.[32])

The particle density and velocity distributions in Fig. 3(a) show the electron accumulation and the low electron velocity behind the barriers. As Fig. 3(a) also shows, the potential profile near the barriers is bent by this nonuniform charge distribution, and this effect is not significant for small $n_e$ ($<10^{17}$ cm$^{-3}$). While the electron energy distribution $dn_e/dE_e$ without a barrier is consistent and close to equilibrium, the low-energy electron density is large in the proximity of the barriers because of low transmission and energy loss by barrier. The phonon energy absorption rate ($\dot{s}_{p\text{-}e} = \dot{S}_{p\text{-}e}/V$, W/m$^3$) is determined by the electron energy distribution ($dn_e/dE_e$), i.e.,

$$\dot{s}_{p\text{-}e} = \sum_j \int_{E_e} [\dot{\gamma}_{p\to e,j}(E_e) - \dot{\gamma}_{e\to p,j}(E_e)] E_{p,j} \frac{dn_e(E_e)}{dE_e} dE_e, \quad (6)$$

where $j$ is an interaction mechanism. Because of the large population at low $E_e$ and no phonon emission with $E_e < E_{p,j}$, the large $\dot{s}_{p\text{-}e}$ is observed near the barriers as in Fig. 3(b).

As shown in Fig. 3(b), the variation of $T_{p,i}$ in simulation region ($<1$ $\mu$m) is rather small ($<1$ K), unless $q_{p,i}$ is extremely large ($>55$ MW/m$^2$), but a rather large difference between $T_{p,LO}$ and $T_{p,A}$ appears near the barriers due to the large $\dot{s}_{p\text{-}e}$. However, since the phonon density ($n_{p,LO} = f_{p,LO}/V_{prim} = 7.56 \times 10^{21}$ cm$^{-3}$ at 300 K, $V_{prim}$ is the primitive cell volume) is more than the four order-of-magnitude larger than $n_e$ ($<10^{17}$ cm$^{-3}$), the depletion of LO phonons is not significant and is quickly made up by upconversion of acoustic phonons (in spite of smaller $\dot{\gamma}_{p\text{-}p}$ than $\dot{\gamma}_{e\text{-}p}$). As phonons are absorbed, $q_p$ (gradient of $T_p$) decreases with $z$, and vanishes when $q_{supply}$ is completely absorbed. This also shows that hot phonons

do not propagate due to the fast relaxation, and therefore, HPAB should be near the hot phonon generation site for high absorption efficiency.

The distribution recovers to equilibrium within a short distance from the barrier (by populating high-energy electrons due to large phonon absorption as well as field acceleration). Unless the electron distribution recovers its population over $\varphi_b$ before the next barrier, large adverse current is induced by this ineffective barrier transition, and therefore, HPAB should have sufficiently large $l_p$ to enable recovery. However, a long $l_p$ leads to larger potential loss through $e_{e,HPAB}$ and needs to be optimized. Phonon absorption must occur at least once to recover the energy loss ($\leqslant E_{p,LO}$), so the required distance can be approximated as $l_p = u_{e,z}\tau_{p\to e,LO}$, where $u_{e,z}$ is the electron velocity in the $z$ direction and $\tau_{p\to e,LO}$ is the time constant of LO phonon absorption ($1/\dot{\gamma}_{p\to e,LO}$), and this increases with $\varphi_b$. Considering an average $u_{e,z} = 1.5 \times 10^5$ m/s (from the isotropic velocity distribution) and $\tau_{p\to e,LO} = 0.4$ ps for equilibrium electrons moving with the forward direction below $E_{p,LO}$, we estimate $l_p = 60$ nm for LO phonon absorption and we choose $l_p = 70$ nm for this work. The MC results also demonstrate that the adverse current by two barriers is almost saturated with $l_p \geqslant 70$ nm and $\varphi_b \leqslant E_{p,LO}$.

The total phonon absorption rate for the HPAB operation ($\dot{S}_{p\text{-}e}/A$, W/m$^2$) is the integration of $\dot{s}_{p\text{-}e}$ over the simulation region, and is almost proportional to $n_e$ (more electrons absorbing more phonons), especially when $n_e$ is low (because of small effect of the charge redistribution). Also, $\dot{S}_{p\text{-}e}/A$ increases with $N_b$ or $\Delta\varphi_g$ due to increase in the transitions (linear proportionality for more than two barriers). So, $\dot{S}_{p\text{-}e}/A$ can be expressed as $a_{p\text{-}e}n_e\Delta\varphi_g$ by introducing the parameter $a_{p\text{-}e}$(A/m). The phonon boost to electrical power per unit area (without current loss) is $P_g = \Delta\varphi_g j_e$. Electrical energy balance in HPAB is

$$\dot{S}_{p\text{-}e}/A - q_e = P_g[= N_b(\varphi_b + e_{e,HPAB}l_p)n_e e_c u_{e,d}], \quad (7)$$
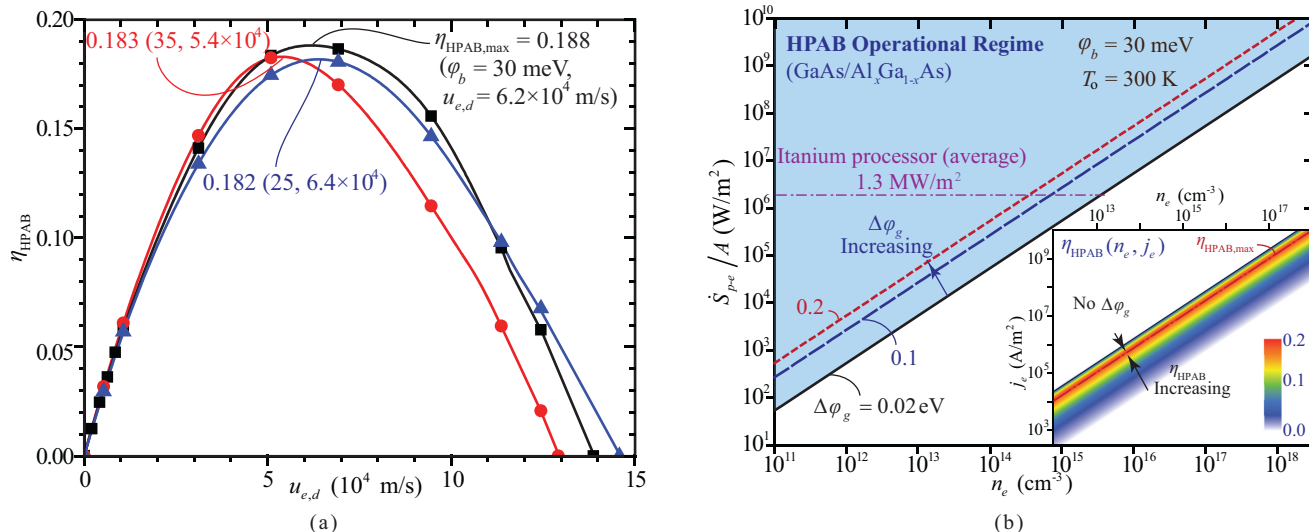
FIG. 4. (Color online) (a) Variations of the HPAB efficiency ($\eta_{HPAB}$) with respect to the drift velocity ($u_{e,d}$). $\eta_{HPAB}$ first increases with $u_{e,d}$ due to increase in the electrical power gain ($P_g = \Delta\varphi_g j_e$) and then decreases because of smaller $\Delta\varphi_g$. The maximum efficiency $\eta_{HPAB,max}$ is 18.8% for $u_{e,d} = 6.2 \times 10^4$ m/s and $\varphi_b = 30$ meV. (b) HPAB operational regime and variations of phonon energy absorption rate $\dot{S}_{p-e}/A$ with respect to $n_e$, for $\Delta\varphi_g = 0.02, 0.1$, and $0.2$ eV, and $u_{e,d} < 10^4$ m/s. Inset shows variations of $\eta_{HPAB}$ with respect to $n_e$ and $j_e$. $\dot{S}_{p-e}/A$ (for $\Delta\varphi_g$ and $j_e$ corresponding to $\eta_{HPAB,max}$) increases with $n_e$.

where $q_e$ is the kinetic energy flux of egressing electrons. Thus, the HPAB efficiency is the ratio of the power gain (electric potential) and the absorbed phonon energy rate,

$$\eta_{HPAB} = \frac{P_g}{\dot{S}_{p-e}/A} = \frac{e_c u_{e,d}}{a_{p-e}}$$

(using $P_g = \Delta\varphi_g e_c n_e u_{e,d}$ and $\dot{S}_{p-e}/A = a_{p-e} n_e \Delta\varphi_g$).

(8)

Higher $u_{e,d}$ yields larger $P_g$, but it also leads to larger potential drop from the increased electric field ($u_{e,d}$ larger than $1.38 \times 10^5$ m/s cannot gain potential with $\varphi_b = 30$ meV), and thus $a_{p-e}$ increases with $u_{e,d}$ (because of smaller $\Delta\varphi_g$). Since the increase in $a_{p-e}$ becomes more pronounced with higher $u_{e,d}$, $\eta_{HPAB}$ has a maximum ($\eta_{HPAB,max}$). $\dot{S}_{p-e}/A$ and $\Delta\varphi_g$ also depend on $\varphi_b$ because higher $\varphi_b$ requires larger $e_{e,HPAB}$ and more phonon absorption per barrier. The simulation results for various $u_{e,d}$ and $\varphi_b$ show that $\eta_{HPAB,max}$ is 18.8% when $u_{e,d} = 6.2 \times 10^4$ m/s and $\varphi_b = 30$ meV, as presented in Fig. 4(a). The phonons are provided by an external source, so higher $\eta_{HPAB}$ is expected by including the phonons emitted in HPAB.

HPAB requires sufficient phonon supply, otherwise phonon depletion reduces $T_{p,LO}$ and the adverse current increases, which in turn results in charge redistribution diminishing the potential gain. The required phonon energy for low $u_{e,d}$ ($<10^4$ m/s) and various $n_e$ and $\Delta\varphi_g$ is estimated by extrapolation from the simulations of low $n_e$ ($=10^{11}$ cm$^{-3}$) with $\varphi_b = 30$ meV and is shown Fig. 4(b). In order for HPAB to operate in a system with larger $n_e$ or $\Delta\varphi_g$, more $\dot{S}_{p-e}/A$ should be provided. The $j_e$ required for high $\eta_{HPAB}$ is selected depending on $n_e$ due to the dominant dependence of $\eta_{HPAB}$ on $u_{e,d}$. ($j_e$ for $\eta_{HPAB,max}$ also increases with $n_e$.) In the conventional electron density ranges ($10^{16}$ to $10^{18}$ cm$^{-3}$), large $\dot{S}_{p-e}/A$ ($>10^6$ W/m$^2$) and $j_e$ ($10^6$ to $10^{10}$ A/m$^2$) are necessary for high $\eta_{HPAB}$, and heat dissipation from some

state-of-the-art integrated processors is in this range.[37] Since HPAB is placed close to phonon source, this is local value at a site (e.g., drain-source channel in high-mobility electron transistors).[38,39]

## IV. CONCLUSIONS

In conclusion, we propose the heterobarrier structure for the direct energy conversion from phonon energy to electric potential. This HPAB combines an abrupt barrier with a gradual potential decrease, which creates favorable conditions for unassisted phonon absorption by increasing the low-energy electron population. The absorbed phonon energy turns into harvestable electric potential without current loss. The HPAB reverses the phonon role, which generally hinders electron transport, by harvesting hot phonons, which would otherwise turn into waste heat.

Through MC simulations, we estimate up to 19% of the phonon energy conversion with proper phonon flux and current. The theoretical efficiency of the HPAB can be estimated by the entropy study and will be discussed in a separate communication. In addition to gaining electric potential (or recovery), integrating HPAB in electronic devices will reduce heat dissipation, lowering operation temperature and enhancing the electron transport (higher mobility) through the effective removal of excess phonons as a heat sink.

## ACKNOWLEDGMENTS

*kaviany@umich.edu

[1] J. N. Fehr, M.-A. Dupertuis, T. P. Hessler, L. Kappei, D. Marti, F. Salleras, M. S. Nomura, B. Deveaud, J.-Y. Emery, and B. Dagens, IEEE J. Quantum Elect. **38**, 674 (2002).

[2] B. K. Ridley, W. J. Schaff, and L. F. Eastman, J. Appl. Phys. **96**, 1499 (2004).

[3] K. T. Tsen, R. P. Joshi, D. K. Ferry, A. Botchkarev, B. Sverdlov, A. Salvador, and H. Morkoç, Appl. Phys. Lett. **68**, 2990 (1996).

[4] P. Kocevar, Physica B **134**, 155 (1985).

[5] A. Matulionis, I. Liberis, I. Matulionien, H. Y. Cha, L. F. Eastman, and M. G. Spencer, J. Appl. Phys. **96**, 6439 (2004).

[6] S. Sakong, P. Kratzer, X. Han, K. Laß, O. Weingart, and E. Hasselbrink, J. Chem. Phys. **129**, 174702 (2008).

[7] A. Goland and A. Paskin, J. Appl. Phys. **35**, 2188 (1964).

[8] G. Conibeer, R. Patterson, L. Huang, J.-F. Guillemoles, D. König a, S. Shrestha, and M. Green, Sol. Energ. Mat. Sol. Cells **94**, 1516 (2010).

[9] X. Ruan and M. Kaviany, ASME J. Heat Transfer **129**, 3 (2007).

[10] J. Kim and M. Kaviany, Appl. Phys. Lett. **95**, 074103 (2009).

[11] P. Santhanam, D. J. Gray, and R. J. Ram, Phys. Rev. Lett. **108**, 097403 (2012).

[12] A. Matulionis, Phys. Status Solidi A **203**, 2313 (2006).

[13] A. Shakouri and J. Bowers, Appl. Phys. Lett. **71**, 1234 (1997).

[14] A. Shakouri, E. Lee, D. Smith, V. Narayanamurti, and J. Bowers, Microscale Thermophys. Eng. **2**, 37 (1998).

[15] R. Kim, C. Jeong, and M. Lundstrom, J. Appl. Phys. **107**, 054502 (2010).

[16] F. Ragay, E. Ruigrok, and J. Wolter, IEEE WCPEC. **2**, 1934 (1994).

[17] Q. S. Zhu, S. M. Mou, X. C. Zhou, and Z. T. Zhong, Appl. Phys. Lett. **62**, 2813 (1993).

[18] M. E. Levinshtein, S. L. Rumyantsev, and M. Shur, *Handbook Series on Semiconductor Parameters* (World Scientific, London, 1996).

[19] M. Kaviany, *Heat Transfer Physics* (Cambridge University Press, Cambridge, 2008).

[20] M. Lundstrom, *Fundamentals of Carrier Transport* (Cambridge University Press, Cambridge, 2000).

[21] S. Egorov and J. Skinner, J. Chem. Phys. **103**, 1533 (1995).

[22] G. P. Srivastava, *The Physics of Phonons* (Adam Hilger, Bristol, 1990).

[23] B. L. Huang and M. Kaviany, J. Appl. Phys. **100**, 123507 (2006).

[24] W. Cai, M. C. Marchetti, and M. Lax, Phys. Rev. B **35**, 1369 (1987).

[25] V. Spagnolo, G. Scamarcio, M. Troccoli, F. Capasso, C. Gmachl, A. M. Sergent, A. L. Hutchinson, D. L. Sivco, and A. Y. Cho, Appl. Phys. Lett. **80**, 4303 (2002).

[26] K. Hess, *Monte Carlo Device Simulation: Full Band and Beyond* (Kluwer Academic Publishers, Dordrecht, 1991).

[27] C. Jacoboni and P. Lugli, *The Monte Carlo Method for Semiconductor Device Simulation* (Springer-Verlag, Berlin, 1989).

[28] C. Moglestue, *Monte Carlo Simulation for Semiconductor Device* (Chapman and Hall, London, 1993).

[29] A. Dargys and J. Kundrotas, *Handbook on Physical Properties of Ge, Si, GaAs and InP* (Science and Encyclopedia Publishers, Vilnius, 1994).

[30] J. Ruch and G. Kino, Phys. Rev. **174**, 921 (1968).

[31] M. Zebarjadi, A. Shakouri, and K. Esfarjani, Phys. Rev. B **74**, 195331 (2006).

[32] K. Kim, K. Hess, and F. Capasso, Appl. Phys. Lett. **52**, 1167 (1988).

[33] T. Luo, J. Garg, J. Shiomi, K. Esfarjani, and G. Chen, Europhys. Lett. **101**, 16001 (2013).

[34] S. Tiwari, *Compound Semiconductor Device Physics* (Academic Press, San Diego, 1992).

[35] D. Vashaee and A. Shakouri, Phys. Rev. Lett. **92**, 106103 (2004).

[36] Z. Bian and A. Shakouri, Appl. Phys. Lett. **88**, 012102 (2006).

[37] F. J. Pollack, in *MICRO'99: Proceedings of the 32nd Annual ACM/IEEE International Symposium on Microarchitecture* (IEEE Computer Society, Washington, DC, USA, 1999), p. 2.

[38] W. Saito, Y. Takada, M. Kuraguchi, K. Tsuda, I. Omura, T. Ogura, and H. Ohashi, IEEE T Electron Dev. **50**, 2528 (2003).

[39] T. Palacios, A. Chakraborty, S. Heikman, S. Keller, S. P. DenBaars, and U. K. Mishra, IEEE Electr. Device L. **27**, 13 (2006).